Transient-response induction detectors for magnetic monopoles: First operation at 78 K

S. Somalwar, H. Frisch, and J. Incandela*
Department of Physics and The Enrico Fermi Institute, The University of Chicago, 5640 South Ellis Avenue, Chicago, Illinois 60637
(Received 5 January 1988)

We have built and tested a small nonsuperconducting magnetic-monopole detector based on Faraday induction. The detector operates at liquid-nitrogen temperature (78 K) and requires only simple steel shielding. It is sensitive to the passage of a Dirac monopole and has uniform velocity response down to the escape velocity from Earth ($v/c=3.8\times10^{-5}$). It consists of a highly resonant copper coil with a simple field-effect-transistor (FET) amplifier, followed by an optimal filter to extract the signal. Measurements of the signal-to-noise ratio agree with calculations for the transient response induced by a monopole on the background of thermal noise. The detector was used to derive a weak upper limit on the magnetic monopole flux. We present a general analysis of such transient response detectors, and discuss the possibility of using high-T_c superconducting loops and FET amplifiers to build a very large array for magnetic-monopole searches sensitive at the Parker limit.

I. INTRODUCTION

The existence of magnetic monopoles is required in all grand unified theories (GUT's) incorporating electromagnetism.[1] To this date, however, theoretical models of the early Universe have predicted a wide range for the monopole flux density in the Universe, with the current opinion being that the flux is small.[2] Our conception of monopoles and of their possible properties and origins has changed radically even in the last few years, and it is possible that there are more such radical changes to come. It thus behooves us to search for such fundamental objects, even if in the present understanding the flux is predicted to be small. The discovery of heavy monopoles would be one of the few ways to observe directly the physics at the grand unified mass scale.

Since the mass scales envisaged in these grand unified theories are many orders of magnitude away from the energies of existing or proposed accelerators,[3] experimenters have returned to the technique of early magnetic monopole searches,[4] trying to observe the monopoles as a component of the cosmic rays. Modern experiments use a wide range of techniques, including ionization in gases[5] and scintillators,[6] and Faraday induction with superconducting elements.[7] In addition, astrophysical limits have been placed on the magnetic-monopole flux assuming monopoles catalyze proton decay.[8]

There is, however, as astrophysical limit which depends less on the assumptions about the monopole properties. The presence of nonzero galactic magnetic fields has been used by Parker[9,10] and his co-workers to set an upper limit on the monopole flux. This limit, on the order of 10^{-15} $cm^{-2}sec^{-1}sr^{-1}$, sets the scale for the next round of monopole search experiments. To be sensitive to a monopole flux near the Parker limit, detectors will have to have surface areas of hundreds of square meters.

No experiment has yet reported a convincing and statistically consistent monopole candidate,[11] although there have been a number of candidates with accompanying periods of excitement.[12] There has been, however, a remarkable growth in the understanding, reliability, and size of both the ionization and induction types of monopole detectors. The ionization of slowly moving protons has been measured at accelerators,[13] and ionization detectors of a size to investigate fluxes at the Parker limit have been and are being built.[14] Faraday-induction detectors have grown by close to an order of magnitude per year for the past several years, and much work has been done in making the detection redundant to avoid the false-signal problems we now understand to be inherent in a single-loop detector.[11,15]

In this work we investigate the Faraday-induction technique in its most general aspects with the goal of understanding whether or not a detector can be built to operate at temperatures above 4 K. All the induction detectors built so far have used superconducting loops at liquid-helium temperature, and the most recent ones also use superconducting quantum interference devices (SQUID's) for current amplification. While superconductivity allows the monopole signal to be dc, it is a fair question to ask whether or not one could detect magnetic monopoles using higher-temperature coils and conventional amplifiers. Such a detector could dispense with the vacuum vessels, superconducting shields required to exclude the change in ambient dc magnetic field, liquid helium, and expensive SQUID's. Nor would it require going underground to avoid the background of cosmic-ray particles.

Previous authors have theoretically addressed the problem of higher temperature induction detectors, and some have concluded that it should be possible to build coils sensitive to the passage of a single Dirac monopole at liquid-nitrogen temperature.[16] Although we have reached the same conclusion, our method for achieving

 ©1988 The American Physical Society

adequate signal-to-noise ratio (S/N) is very different. In this paper we describe the theoretical basis for our conclusion and the experimental measurements. Finally, a direct measurement of the S/N is presented.

The long-term goal of this development is to build a very large area (many hundreds of square meters) induction detector for magnetic monopoles. One way to use the transient detection technique we describe here is to make a large array of several layers, each layer consisting of many individual coils. The signal would then consist of a straight "track" through coils in different layers. As will be seen, nonsuperconducting copper coils are limited in size due to S/N considerations, so that it would take a large number of coils to make a reasonable size detector. It is not yet clear which is cheaper: the large superconducting loops with orthogonal gradiometers for redundancy, but with vacuum vessels, shields, and SQUID's; or many small liquid-nitrogen temperature copper coils with relatively inexpensive field-effect-transistor (FET) amplifiers. It may turn out that a "hybrid" solution, namely, superconducting coils with FET readout, is the most practical one. In light of the recent breakthrough in the field of high-critical-temperature superconductors,[17] it may be possible to build the superconducting output coils at liquid-nitrogen temperature. Because of the current rapid pace of evolution of high-temperature superconductor technology we do not attempt any economic comparisons, but limit ourselves to the fundamental questions of how the signal is extracted, what kind of shielding is adequate, what S/N we have been able to achieve with liquid-nitrogen temperature copper coils, and the improvements we expect with superconductor input loops.

The organization of this paper is as follows. In Sec. II, we evaluate the response of a general Faraday-induction detector to magnetic monopoles of arbitrary velocity. Section III describes the transient-voltage detection scheme. It is shown that the signal is dominated by the thermal-noise background, and a filtering process to increase the signal-to-noise ratio is introduced. The nature of the filter suggests an optimal design strategy for the detector, and is described in Sec. IV. The signal-to-noise ratio for the copper coil used in a prototype detector is also calculated in the same section. The prototype itself is described in Sec. V. Section VI describes the calibration procedure, the results from a short detector run and an estimate of the false-event probability for the attained signal-to-noise ratio. Finally, a brief discussion of the transient-detection technique with superconducting input coil follows in Sec. VII. The appendixes are used to describe the current detector scheme, the design of low-loss coils, and a method of measuring the quality factor of a very-low-loss coil.

II. MONOPOLE emf AND VELOCITY RESPONSE

Consider a monopole with magnetic charge g and nonrelativistic velocity v passing along the axis of a loop with radius a and having n number of turns. The induced electric field $\mathbf{E}$ is given by Faraday's law of induction generalized to include the magnetic current:

$$\nabla\times\mathbf{E}+\frac{1}{c}\frac{\partial\mathbf{B}}{\partial t}=-\frac{4\pi}{c}\mathbf{j}_m \quad \text{(cgs units)} . \tag{1}$$

Assuming that the monopole crosses the plane of the loop at time $t=0$, the induced emf, $e_m(t)$, is calculated from Eq. (1) as

$$e_m(t)=\frac{2\pi ngv/a}{[1+(v^2/a^2)t^2]^{3/2}} \quad \text{(SI units)} . \tag{2}$$

By taking the Fourier transform of Eq. (2) we can study the induced emf as a function of the frequency. It is

$$e_m(\omega)=4\pi ng\left[\frac{\omega}{v/a}\right]K_1\left[\frac{\omega}{v/a}\right] , \tag{3}$$

where K_1 is the modified Bessel function of order 1. The ratio a/v is the characteristic time scale of the system and hence v/a is the frequency scale. Knowing the characteristic frequency, one can label the frequencies by the dimensionless ratio $x=\omega/(v/a)$. The function $xK_1(x)$ is very flat for small x ($x \ll 1$) and decays exponentially for large x ($x \gg 1$). This behavior is seen in the square of the emf shown as a function of frequency in Fig. 1. The half emf point occurs for

$$\frac{\omega}{v/a}=1.26 .$$

The characteristic frequency is given by the ratio of the monopole velocity to the loop radius. The monopole velocity response for a loop with known radius can be obtained from Fig. 1. As an example, consider a 10-cm-diameter detector operating below 10 kHz, i.e., the upper

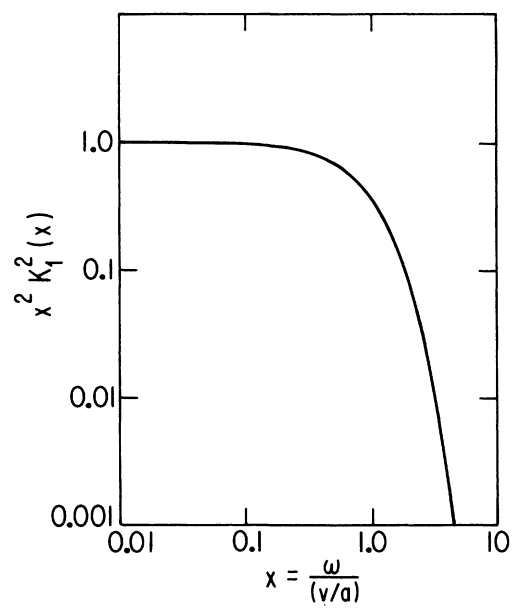

FIG. 1. The square of the calculated normalized monopole emf per unit frequency $[xK_1(x)]^2$ plotted versus the normalized frequency $x=\omega/(v/a)$. The diameter of the coil is a and the monopole velocity is v. $K_1(x)$ is the modified Bessel function of first order.

cutoff frequency of the detector is 10 kHz. All monopoles with velocity in excess of $8.3\times10^{-6}c$ (2.5 km/sec) have half emf point above the upper cutoff frequency. Thus, the detector is fully effective in detecting monopoles traveling faster than $8.3\times10^{-6}c$. Conversely, the same criterion can be used to decide the upper cutoff frequency for a given size detector so that it remains sensitive to all monopole velocities above a certain threshold. For example, in order to detect a monopole falling freely to Earth ($v\sim3.8\times10^{-5}c$, the escape velocity) a 10-cm-diameter detector must operate below an upper cutoff frequency of 46 kHz, i.e., in the full power frequency region.

Throughout the paper we shall assume that the detector under discussion has been designed to operate below the upper cutoff frequency, i.e., in the full power frequency region. Hence, the monopole emf in Eq. (3) is taken to be independent of the frequency:

$$e_m(\omega)=4\pi ng \ . \tag{4}$$

A Dirac monopole then induces 4.14×10^{-15} V sec per turn, which is a very small number.

So far we consider monopoles with trajectories along the loop axis. For off-axis trajectories, the effective radius of the loop appears smaller and as a result, the fast monopole approximation [Eq. (4)] is even better.

To be able to detect the signal, the emf calculated above has to be converted into either a voltage or a current. One method of achieving this conversion would be to connect the loop as the input to a low noise amplifier and to analyze the amplifier output for a monopole signal. Two types of amplifiers can be used for this purpose. A voltage amplifier can amplify the voltage across the shunt capacitance. An ideal voltage amplifier has zero input noise and infinite input impedance, and is best approximated by an FET. Alternatively, a current (transimpedance) amplifier can be used to short-circuit the capacitance and amplify the current produced by the inductance. An ideal current amplifier has zero input noise and zero input impedance. It is well approximated by a low noise inverting operational amplifier with noiseless feedback and also by a SQUID. All the cosmic-ray monopole induction detectors built so far have used SQUID's for current amplification. The analyses of both the voltage and current amplification schemes are very similar. However, for amplifiers with equivalent intrinsic performance, the signal-to-noise ratio in the voltage case is always superior to that in the current case. The current detector scheme is discussed in Appendix A.

III. SIGNAL DETECTION AND NOISE

Figure 2 shows the equivalent circuit of a sensing coil connected to a voltage amplifier. The coil has n turns, inductance L, and resistance $R(\omega)$ at frequency ω. The shunt capacitance C includes the coil-winding capacitance, amplifier input capacitance, and any external tuning capacitance. The amplifier has gain $G(\omega)$ at frequency ω. Let e_m be the monopole emf as calculated above, e_t be the coil thermal (Johnson) noise, and e_n and i_n denote the amplifier voltage and current noise, respectively. The

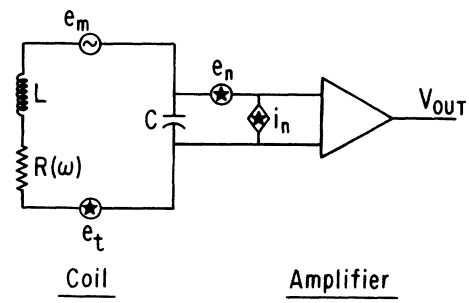

FIG. 2. The equivalent circuit of a voltage sensing detector. The input coil has inductance L, resistance $R(\omega)$, and capacitance C. The amplifier output $V_{\rm out}$ is proportional to the voltage across the capacitance. e_m is the monopole emf and e_t the coil thermal noise. e_n and i_n denote the amplifier voltage and current noise, respectively.

monopole signal voltage $M(t)$ at the amplifier input is then a solution of the differential equation:

$$LC\frac{d^2M(t)}{dt^2}+RC\frac{dM(t)}{dt}+M(t)=e_m(t) \ . \tag{5}$$

The Fourier transform then gives the signal in frequency space:

$$M(\omega)=\frac{4\pi ng}{1-(\omega/\omega_0)^2+[i/Q(\omega)](\omega/\omega_0)^2} \qquad (-\infty<\omega<\infty) \ , \tag{6}$$

where ω_0 is the coil resonant frequency $[\omega_0=(LC)^{-1/2}]$ and $Q(\omega)$ is the coil quality factor $[Q(\omega)=\omega L/R(\omega)]$. Note the strong peaking of the signal at the resonant frequency, characteristic of an RLC circuit set into oscillation. To get an idea of what the signal looks like in the time domain we assume that the coil resistance $R(\omega)$ is a slowly varying function of frequency and hence can be taken to be a constant $[R(\omega)\sim R]$. Then, define $Q_0=\omega_0L/R$ and take the inverse Fourier transform of Eq. (6) to get the signal in the time domain

$$M(t)=\begin{cases}0, & t\le0 \ ,\\ 4\pi ng\,\omega_0 e^{-\omega_0 t/2Q_0}\sin(\omega_0 t), & t\ge0 \ .\end{cases} \tag{7}$$

The decaying sinusoid is the RLC response to a step input. The discontinuity in the first derivative at monopole crossing time ($t=0$) is a remnant of the (harmless) fast-monopole approximation we made above.

The signal voltage has to be discriminated from a background thermal voltage noise generated by the coil resistance and from the input noise of the amplifier. To estimate the signal-to-noise ratio for monopole detection, the noise-power spectral density $S_n(\omega)$ is needed. $S_n(\omega)$ is the sum of three independent terms:

$$S_n(\omega)=S_{nt}(\omega)+S_{nv}(\omega)+S_{ni}(\omega) \ , \tag{8}$$

where $S_{nt}(\omega)$, $S_{nv}(\omega)$, and $S_{ni}(\omega)$ are the spectral densities of the coil thermal noise, amplifier voltage noise, and the voltage due to the amplifier current noise, respectively.

The first term on the right-hand side of Eq. (8) comes from the Johnson noise[18] spectrum $2kTR(\omega)$ of the coil resistance $R(\omega)$ maintained at temperature T (k is the Boltzmann constant). The spectrum gets modified by the coil RLC response given by the absolute value squared of the denominator in Eq. (6) and we have

$$S_{nt}(\omega)=\frac{2kTR(\omega)}{[1-(\omega/\omega_0)^2]^2+[1/Q^2(\omega)](\omega/\omega_0)^4} \quad (-\infty<\omega<\infty) . \tag{9}$$

For the special case of $R(\omega)=\text{const}$, it is easy to verify that Eq. (9) conforms to the statment of the equipartition theorem

$$\frac{1}{2\pi}\int_{-\infty}^{\infty} S_{nt}(\omega)d\omega=\frac{kT}{C} . \tag{10}$$

Note that in the limit of infinite resonant frequency (i.e., the RLC circuit being replaced by a resistor R), Eq. (9) gives back the familiar white noise expression

$$S_{nt}(\omega)=2kTR(\omega) \quad (\omega_0\to\infty)(-\infty<\omega<\infty) . \tag{11}$$

The second term on the right-hand side of Eq. (8) is the amplifier input voltage noise density, $S_{nv}(\omega)$. It is device dependent, unaffected by the RLC response, and is flat as a function of frequency. We denote the amplifier noise voltage spectral density by $\lambda_v(\omega)$. As an example, an amplifier with input noise of 1 nV/$\sqrt{\text{Hz}}$ has spectral density of[18]

$$\lambda_v(\omega)=\tfrac{1}{2}(10^{-9})^2 \text{ V}^2\text{sec} =5\times10^{-19} \text{ V}^2\text{sec}, \quad -\infty<\omega<\infty .$$

Then,

$$S_{nv}(\omega)=\lambda_v(\omega), \quad -\infty<\omega<\infty . \tag{12}$$

The last term in Eq. (8), $S_{ni}(\omega)$, is the amplifier current noise density. We denote the noise current spectral density by $\lambda_i(\omega)$. For example, 1 fA/$\sqrt{\text{Hz}}$ noise current specification translates to[18]

$$\lambda_i(\omega)=\tfrac{1}{2}(10^{-15})^2 \text{ A}^2\text{sec} =5\times10^{-31} \text{ A}^2\text{sec}, \quad -\infty<\omega<\infty .$$

The noise current of the input device causes a voltage drop across the RLC impedance of the source circuit, which is seen as another contribution to the input noise:

$$S_{ni}(\omega)=\frac{\lambda_i(\omega)R^2(\omega)[1+Q^2(\omega)]}{[1-(\omega/\omega_0)^2]^2+[1/Q^2(\omega)](\omega/\omega_0)^4} , \quad -\infty<\omega<\infty . \tag{13}$$

Combining all the noise term [Eqs. (9), (12), and (13)] we get the total input noise voltage spectrum:

$$\begin{aligned} S_n(\omega)&=\frac{2kTR(\omega)+\lambda_i(\omega)R^2(\omega)[1+Q^2(\omega)]}{[1-(\omega/\omega_0)^2]^2+[1/Q^2(\omega)](\omega/\omega_0)^4}+\lambda_v(\omega) \\ &=2kTR(\omega)\left[\frac{1+\eta(\omega)[1+Q^2(\omega)]}{[1-(\omega/\omega_0)^2]^2+[1/Q^2(\omega)](\omega/\omega_0)^4}+\chi(\omega)\right], \quad -\infty<\omega<\infty , \end{aligned} \tag{14}$$

where the dimensionless quantities $\eta(\omega)$ and $\chi(\omega)$ denote the ratios of the amplifier current noise and voltage noise to the coil noise, respectively:

$$\eta(\omega)=\frac{\lambda_i(\omega)R(\omega)}{2kT}, \quad \chi(\omega)=\frac{\lambda_v(\omega)}{2kTR(\omega)} . \tag{15}$$

Now we are in a position to compare the signal [Eq. (6)] with the noise [Eq. (14)]. For the sake of simplicity we initially ignore the amplifier noise [$\eta(\omega)=\chi(\omega)=0$] and assume that $R(\omega)$ is independent of ω. Then, the signal is a decaying sinusoid [Eq. (7)] and the noise is given by the equipartition theorem [Eq. (10)]. The power signal-to-noise ratio (S/N), defined as the maximum signal amplitude squared divided by the mean-squared noise amplitude, is

$$S/N=\frac{(4\pi g)^2}{kT}\left[\frac{n^2}{L}\right] . \tag{16}$$

For coils with fixed shape, n^2/L is a decreasing function of the coil size falling approximately as the inverse of the radius.[19] Thus the S/N is independent of the number of turns and decreases as the coil size increases. For a 100-cm^2 (11.4-cm-diameter) solenoid with length equal to radius, $L/n^2=0.12\times10^{-6}$ H. The S/N at liquid-nitrogen temperature (78 K) is 0.14, which is clearly inadequate.

However, the S/N in Eq. (16) does not express our full knowledge of the signal and noise. Since the spectra for both are known completely, some way of converting the spectral information into enhanced signal amplitude would boost the signal in comparison with the noise. It is well known in the theory of linear filters[20] that the best way to extract information is to pass the data through an optimal filter given by $K(\omega)=M^*(\omega)/S_n(\omega)$ where $M(\omega)$ is the signal Fourier transform and $S_n(\omega)$ is the noise spectral density. The concept of optimal filtering can be understood in several different ways. Physically, one can think of looking for an occurrence of the signal embedded in the noise background by scanning with a template. Clearly, the chances of locating the signal are greatly improved if the template looks more like the signal and less like the noise. The mathematical interpreta-

tion of the filter is more intuitive in the frequency domain—the optimal filter gives more weight to the frequency regions where the signal exceeds the noise compared to the regions where the reverse is true.

The filter can also be explained on the basis of information theory. Consider an example where a very small signal is buried in a large incoherent background of random sinusoidal noise. If the signal itself were also sinusoidal, it would be harder to locate its occurrence than if it were, say, a step signal. It is easier to locate the step signal because its (spectral) shape differs from that of the noise and as such, there is more information available. A filter that takes into account the difference in shape of the signal and noise is obviously more efficient at searching for the signal. Equivalently, such a filter utilizes information available by way of the known difference in shapes to increase the filtered signal amplitude in comparison with the filtered noise. The optimal filter squeezes out all of the available shape information from its input to increase the signal size. At the output of the filter, the signal gets a maximum possible boost in size, but the signal and noise acquire identical spectral shapes. One can thus derive the expression for the optimal filter in a one-line calculation by requiring the output signal and noise to have the same spectral shape, or in other words, to be proportional in the frequency space $[M(\omega)K(\omega) = S_n(\omega)\,|K(\omega)|^2]$. The maximum possible S/N using the optimal filter is given by

$$S/N = \frac{1}{\pi}\int_0^\infty \frac{|M(\omega)|^2}{S_n(\omega)}d\omega \ . \tag{17}$$

Using $M(\omega)$ from Eq. (6) and the full noise spectrum from Eq. (14), we find the S/N in the voltage sensing scheme to be

$$S/N = \frac{(4\pi g)^2}{kT}\left[\frac{L}{n^2}\right]^{-1} G_{\text{opt}} \ , \tag{18}$$

where G_{opt} is the gain in the S/N due to the optimal filter:

$$G_{\text{opt}} = \frac{1}{2\pi}\int_0^\infty Q(\omega)\frac{d\omega/\omega}{1+Q^2(\omega)\eta(\omega)+[1-(\omega/\omega_0)^2]^2\chi(\omega)} . \tag{19}$$

We have ignored terms of the order $Q^{-2}(\omega)$ in the denominator because $Q \gg 1$. Each term in the integrand of Eq. (19) can be ascribed a physical meaning. Higher values for $Q(\omega)$ in the numerator means a larger number of cycles in the signal due to the lower loss per cycle and hence a higher information content in the signal. The three terms in the denominator are scaled to the coil noise, and represent the coil resistance, amplifier current, and amplifier voltage noise, respectively.

If one assumes that the amplifier noise is negligible and that the resistance $R(\omega)$ is a constant, the signal-to-noise ratio given by Eq. (18) becomes infinitely large. Although the assumptions may be technically hard to achieve, they are not unphysical. The divergence is a result of the fast monopole velocity approximation. An infinitely fast monopole deposits energy in the entire frequency band, and a noiseless amplifier can then extract it from the entire band. In practice, the amplifier has wideband noise which prevents it from accessing the entire range of frequencies, thus curing the divergence. Because of the frequency cutoff, all the monopoles above a certain velocity are guaranteed to have the same response. As before, a monopole traveling with bare terrestrial escape velocity and a relativistic monopole will both induce the same signal in a 10-cm-diameter loop provided the detector operates below 46 kHz.

IV. MAXIMIZING THE SIGNAL-TO-NOISE RATIO

Let us combine Eqs. (18) and (19) to obtain the complete expression for the signal-to-noise ratio

$$S/N = \frac{(4\pi g)^2}{kT}\frac{n^2}{L}\frac{1}{2\pi}\int_0^\infty \frac{Q(\omega)}{\omega}\frac{d\omega}{1+Q^2(\omega)\eta(\omega)+[1-(\omega/\omega_0)^2]^2\chi(\omega)} . \tag{20}$$

A very low noise current level can be achieved using an FET for the input stage of the amplifier. In that case, the current noise term $Q^2(\omega)\eta(\omega)$ can be ignored. Since $Q = \omega L/R$, Eq. (20) can be rewritten as

$$S/N = \frac{(4\pi g)^2}{kT}\frac{n^2}{L}\frac{1}{2\pi}\int_0^\infty \frac{L}{R(\omega)}\frac{d\omega}{1+[1-(\omega/\omega_0)^2]^2\chi(\omega)} . \tag{21}$$

The following procedure is then used to compute the S/N. First, the Q of the coil is measured as a function of frequency (see Appendix C), from which one can calculate the total coil resistance $R(\omega)$ as a function of frequency. Knowing the amplifier noise parameters, the function $\chi(\omega)$ is calculated. The S/N is then obtained by numerically computing the integral in Eq. (21).

In order to maximize the S/N, we shall scrutinize each term in Eq. (21). The monopole charge g is fixed. It is desirable to lower the operating temperature T as much as possible so as to reduce the thermal noise contribution from the coil. The term n^2/L is purely geometric and is inversely proportional to the radius for coils with same shape. Hence, the loop size should be small. A low noise amplifier is required to increase the S/N. The last and most important term in the equation for the S/N is the resistive loss. The lower the coil loss, the longer is the duration of its oscillatory response to the monopole. A

low-loss coil maximizes the SNR by retaining more information about the monopole passage. If we ignore the amplifier noise, Eq. (21) shows that for coils with the same size and shape, the SNR is directly proportional to the integrated quality factor $\langle Q \rangle$ of the coil defined by

$$\langle Q \rangle = \int_0^\infty \frac{L}{R(\omega)} d\omega \ . \tag{22}$$

In the context of S/N maximization, the appropriate meaning of the phrase "low-loss coil" is that the coil has high $\langle Q \rangle$. For our application, the unsolved problem of designing a coil to have high Q at a given frequency is compounded since low loss is required over a wide frequency range to increase the S/N. Appendix B contains a summary of our work on this subject. Equation (21) gives us the recipe for designing a transient detector for a given low-loss copper coil. In the rest of this section we will illustrate the design recipe by calculating the maximum possible S/N for an actual high $\langle Q \rangle$ copper coil.

Figure 3 shows the measured Q as a function of frequency for a 15-layered 11.4-cm-diameter copper coil with 288 turns per layer at 50.4 turns per cm winding pitch. The wire diameter was 0.127 mm (American Wire Gauge No. 36). The layers were separated by 0.76-mm-thick polyethylene dielectric spacer. The coil was maintained at 78 K temperature by submerging in liquid nitrogen. If the coil did not develop any ac resistance, the graph would be a straight line shown in the figure. The coil inductance L and internal capacitance C_{int} are measured to be 2.313±0.002 H and 42.1±1.2 pF, respectively. Knowing the inductance, the function $R(\omega)$ for the coil is calculated using the definition $Q(\omega)=\omega L/R(\omega)$. The top curve in Fig. 4 is the plot of $L/R(\omega)$ against frequency. The same curve can also be interpreted as the integrand on the right-hand side of Eq. (21) for a noiseless amplifier. The lower curve in Fig. 4 shows the same integrand as a function of frequency for this coil assuming 1 nV/$\sqrt{\text{Hz}}$ amplifier noise. The detector frequency ω_0 in the integrand was chosen to maximize the area under the lower curve, or in other words, to maximize the signal-to-noise ratio (S/N). When $\omega=\omega_0$, the amplifier noise term in the denominator of Eq. (21) is zero, and the S/N integrand becomes the same as the integrand for the case of a noiseless amplifier. As a result, the two curves touch each other when $\omega=\omega_0$.

Finally, Fig. 5 shows the maximized S/N for a Dirac monopole as a function of the amplifier noise for the coil. Next we describe the prototype we developed to test the performance of this coil as a monopole detector. Then we will compare the observed S/N with the expected S/N from Fig. 5.

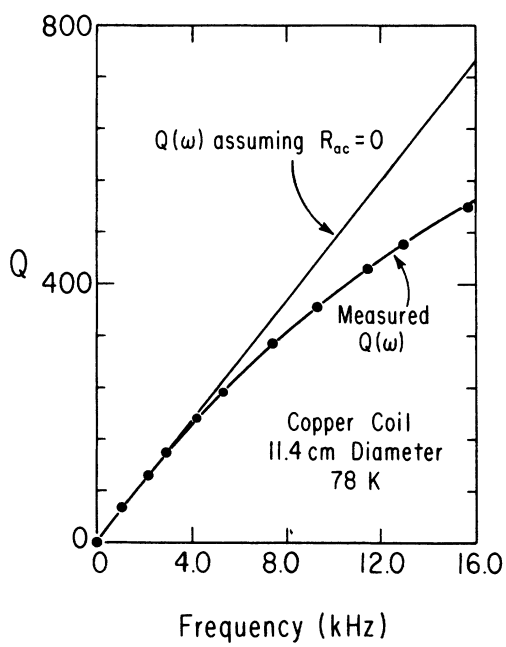

FIG. 3. The measured quality factor Q as a function of the frequency for a 11.4-cm-diameter copper coil at 78 K. The coil has 288 turns of 0.127-mm-diameter wire per layer. The solid curve is a fit assuming a power law for the ac resistance (see Appendix B). If the coil did not develop any ac resistance, the graph would be a straight line as indicated.

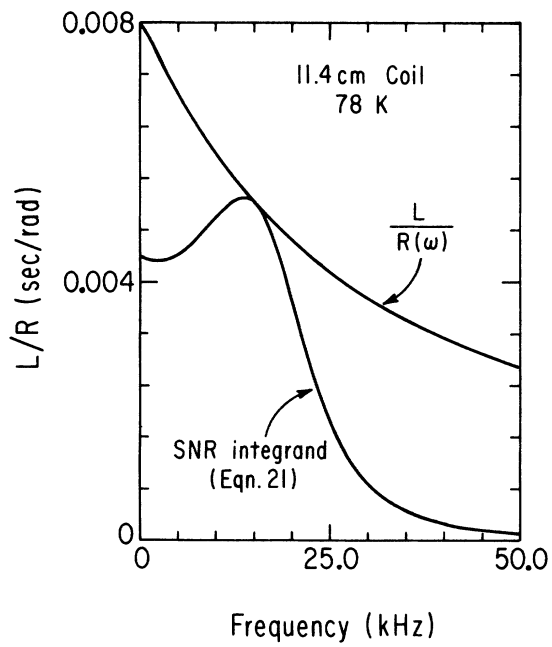

FIG. 4. The integrand of the predicted S/N as a function of frequency for the coil of Fig. 3. For a noiseless amplifier (top curve), the integrand is the ratio $L/R(\omega)$, where L is the coil inductance and $R(\omega)$ is its resistance. For an amplifier with 1 nV/$\sqrt{\text{Hz}}$ input noise (lower curve), the ratio is modified to take into account the noise in accordance with Eq. (21).

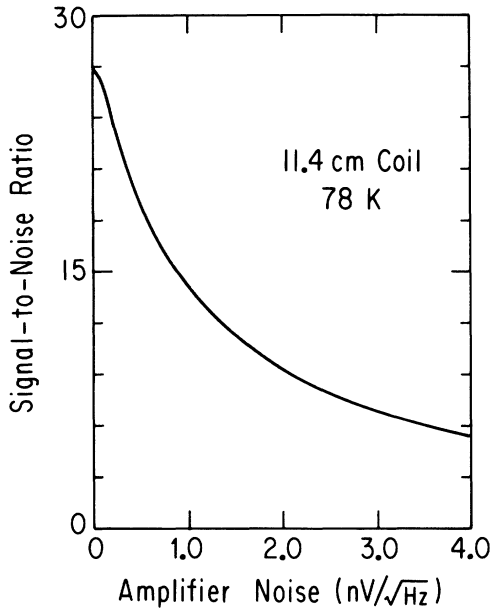

FIG. 5. The estimated (power) signal-to-noise ratio for the copper coil of Fig. 3 as a function of the amplifier noise. The coil is cooled to 78 K. The measured values of the coil Q at different frequencies (Fig. 3) are used in the estimation.

V. PROTOTYPE DEVELOPMENT

The prototype (Fig. 6) consists of a jacketed steel housing for the coils, which is attached to an aluminum box containing the amplifier and the calibration drive circuit. The two 3.2-mm-thick layers of steel shield the coil from the ambient ac electromagnetic field. The volume between the steel layers holds liquid nitrogen. The whole assembly is thermally insulated by a thick coating of polyurethane form and a vapor barrier to minimize boiloff. Steel tubes with tight fittings act as shielded conduits for the leads from the coil to the amplifier box. The input coil is mounted on a support plane suspended from the top of the steel box with G-10 rods. The support plane is made of reconstituted strengthened wood. The amplifier box is made of 3.2-mm-thick aluminum and shields the low-noise amplifier card. The power supply lines into the amplifier box are filtered at the connectors, and the amplifier section power supply is completely decoupled from that of the calibration circuit.

The detection sensitivity of the coil is measured using a "pseudopole." This is a toroidal calibration solenoid made by winding thin wire on flexible nonmetallic tubing. The calibration is done by passing a measured step function current through the solenoid. The step causes a change in the magnetic flux linked to the coil, thereby mimicking the passage of a monopole. Since the pseudopole is metallic, one has to guard against the possibility of Q degradation of the detector coil due to eddy loss. Hence, two precautions were taken while designing the pseudopole. First, very resistive thin wire (Evanohm, for example) is used to wind the pseudopole. Second, the pseudopole is made as small as possible without introducing a significant wire diameter correction in the calibration. Lower metal volume results in lower eddy loss. There is an added benefit in making the pseudopole small. The larger the diameter of the solenoid, the smaller is the current step required to mimic a monopole. Since the flux change required to mimic a monopole is very small, and a small current flux is hard to regulate and measure, a smaller pseudopole results in smaller calibration error. For the pseudopoles we built, one monopole current step was determined to be $(24.9\pm1.5)\times10^{-9}$ A. The current step is generated by cascading low-noise amplifiers with gains less than unity in series and applying the output voltage across the known resistance of the pseudopole.

The coil output is amplified by an ultralow-noise FET input cascode amplifier shown in Fig. 7. The cascode configuration keeps the input capacitance of the amplifier to a minimum by eliminating the Miller effect. The amplifier output is passed through the combination of an 8-pole active Butterworth high-pass filter centered at 250 Hz and an 8-pole active Butterworth low-pass filter at 47 kHz. The high-pass filter attenuates the unavoidable 60-Hz line frequency and the low-pass filter provides the guard band to prevent aliasing[21] in digitization. The filter output is digitized using a Data Translation[22] DT3362 12-bit analog-to-digital system and the data is then written in units of 512 byte buffers to magnetic tape. The analog to digital conversion of the data was done in the burst mode of the A/D converted by clocking it externally at the rate of 125 kHz. Since the coil output is very narrowly peaked at its resonant frequency, the external clock must be very stable over the digitization interval. A 1.0-MHz quartz-crystal oscillator clock with a 4-bit TTL binary counter in "divide by eight" configuration was used. Several sets of data files were collected with pseudopole excitation of different strengths starting from zero up to 20 Dirac monopoles. The data were then transferred on magnetic tapes to a Digital VAX-8600 for off-line analysis.

VI. DATA ANALYSIS

The signal-to-noise ratio in the raw data is expected to be low. To extract the signal from the noise, the data has to be passed through the optimal filter of Sec. III given by

$$K(\omega)=M^*(\omega)/S_n(\omega)\ , \tag{23}$$

where $M(\omega)$ is the signal Fourier transform and $S_n(\omega)$ is the noise spectral density. Since the digitized data is discrete, we need the discrete realization of the continuous filter $K(\omega)$. The realization is done in the time domain by expressing the filter output stream M_l^{out} as a discrete convolution of the input stream M_l^{in} and the transverse optimal filter K_l

$$M_l^{\text{out}}=\sum_{k=-\infty}^{\infty} M_k^{\text{in}}K_{l-k}\ , \tag{24}$$

where K_l is the inverse Fourier transform given by

$$K_l=\frac{1}{2\pi}\int_{-\pi}^{\pi} d\omega\, K(\omega)e^{il\omega}\ . \tag{25}$$

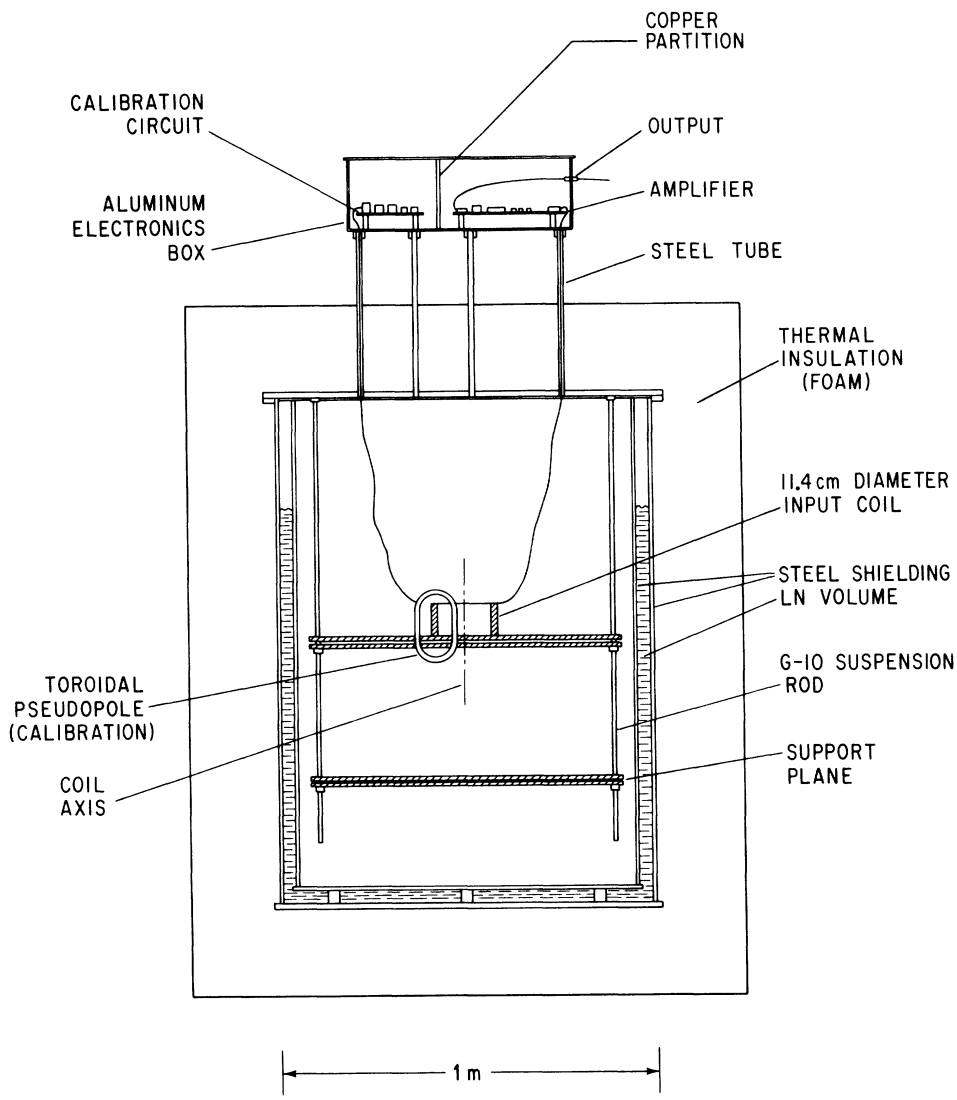

FIG. 6. The prototype transient detector. The copper sensing coil is cooled to 78 K by the liquid nitrogen contained between the two layers of the electromagnetic steel shielding. The signal voltage is amplified by the low-noise FET amplifier housed in an aluminum box with the calibration drive circuit. The detector is calibrated using a toroidal solenoid threading the coil. The output of the amplifier is digitized.

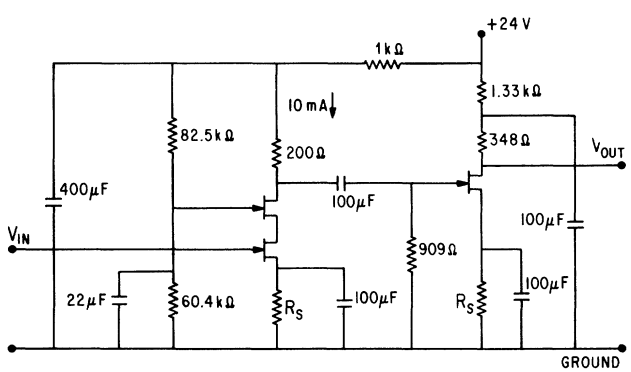

FIG. 7. The first two stages of the low-noise high-input-impedance amplifier. The input stage is in an FET cascode configuration to avoid the Miller effect capacitance. Extensive *RC* filtering is used to eliminate the power line noise and decouple the stages. The first stage operates at high drain current (10 mA) in order to keep the input noise level low.

The limited bandwidth in the integral is due to the finite-sampling frequency during digitization (Nyquist theorem).

The data with calibration signals of various strengths was optimally filtered to improve the signal-to-noise ratio. The response of the detector for a given calibration strength was determined by averaging over a number of repeated calibration signals. Figure 8 is the calibration curve for the detector. It shows the ratio of the average signal strength to the root-mean-squared noise plotted as a function of the calibration strength. The graph is a straight line as expected. The negligibly small intercept indicates the lack of stray parasitic coupling between the monopole detection circuit and the preattenuation high-level pseudopole excitation voltage. From the calibration curve, the power signal-to-ratio (S/N) for a single Dirac charged monopole can be read out to be 25.9. There is a 12% error on this S/N figure. The error is entirely due

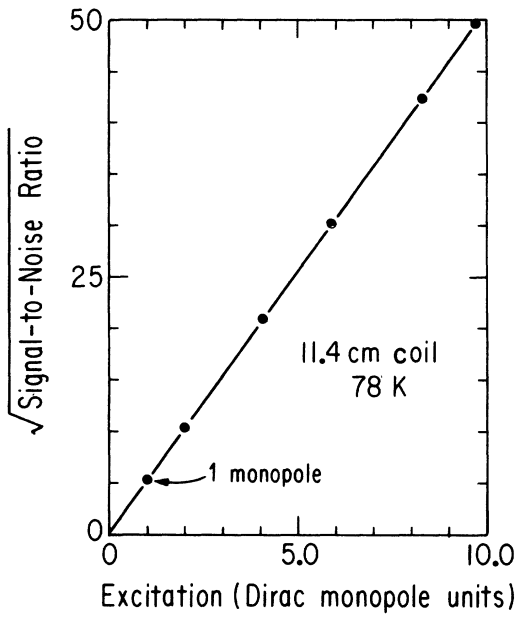

FIG. 8. Detector calibration results: the square root of the measured signal-to-noise ratio as a function of pseudopole excitation for the 11.4-cm copper coil of Fig. 3. Note that the detector is sensitive to the passage of a single Dirac monopole.

to the 6% uncertainty in the estimate of the pseudopole calibration current. Thus, the S/N for a Dirac monopole is measured to be 25.9 ± 3.1.

Knowing the coil resistance as a function of frequency, one can calculate the S/N expected for a Dirac monopole [see Eq. (21)]. The calculated value of S/N for the detector is 20.6 ± 6.2. The large 30% error in the calculated S/N is from the 15% error due to the extrapolation of the coil ac resistance beyond the coil self-resonance frequency. The calculated value of 20.6 ± 6.2 compares favorably with the measured value of 25.9 ± 3.1 above.

Figure 9(a) shows a sample stretch of raw data. Although it is not evident to the eye, it contains a signal equivalent to a single Dirac monopole at the location marked by the arrow. Figure 9(b) shows the same stretch of data after processing with the optimal filter. The signal is seen clearly in the processed data. The full width at half maximum of the signal is measured to be $(15.2\pm0.1)\times10^{-6}$ sec. In order to evaluate the noise-induced false event rate, a long (0.9 sec) stretch of noise data was taken and passed through the optimal filter. The output was then analyzed for excursions above different values of the threshold and the result was histogrammed. Since the thermal noise is Gaussian and all the filtering is linear, the processed noise is also expected to obey Gaussian statistics. The goodness of the Gaussian fit in the excursion histogram in Fig. 10 demonstrates that the output is indeed Gaussian. For the prototype detector, the mean time between any noise excursion above the Dirac monopole level is expected to be approximately 8 sec without coincidence requirement. With a two-loop coincidence detector, it goes down to once in 112 days. With triple coincidence, the rate should be approximately one signal per 320 000 years, which is negligibly small. (Although many such detectors would operate at the same time, thereby reducing the effective lifetime.) We obtained an upper limit of 1.7×10^{-3} $cm^{-2}sr^{-1}sec^{-1}$ on the Dirac monopole flux by running our detector without coincidence requirement for 0.9 sec.

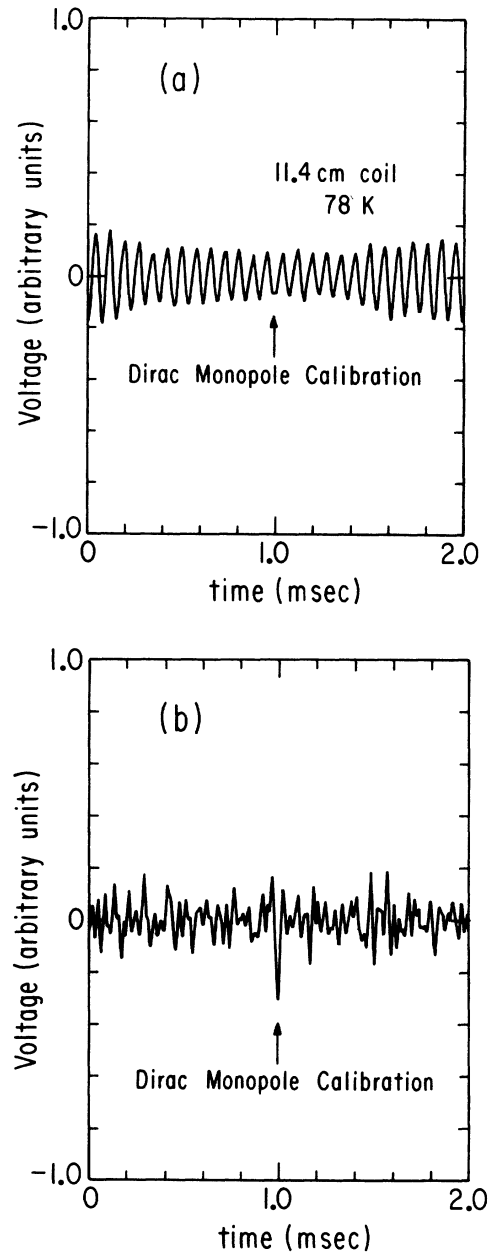

FIG. 9. (a) A simple stretch of the detector output containing calibration signal equivalent to one Dirac monopole at the location shown by the arrow. The signal is washed out by the thermal noise of the coil. Note that the background thermal noise is almost purely sinusoidal indicating a highly resonant coil. (b) After optimal filtering, the same data shows the one monopole calibration clearly at the location marked by the arrow. The data is no longer sinusoidal. The filtering process completely eliminates the resonant frequency component. The time resolution of the detector is obtained by measuring the full width at half maximum of the signal.

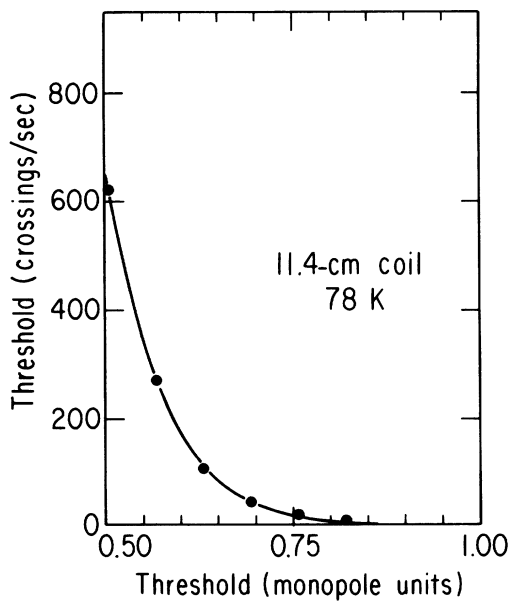

FIG. 10. The measured noise-induced false-event rate as a function of the signal threshold expressed in units of a single Dirac monopole. The data from a single 11.4-cm coil (Fig. 3) was recorded without any calibration signals, filtered, and scanned for noise-voltage excursions above a present threshold level. Since the noise is Gaussian, the error function fit approximates the data very well. The mean time for a noise-induced one monopole signal is calculated from the fit coefficients to be approximately 8 sec.

Given the mean event rate of one per 8 sec, the probability of observing no noise-induced event is 90% for 0.9-sec running time. In other words, at 90% confidence level, zero false events are expected to occur in that interval. Poisson statistics is used in calculating these probabilities.

The two layers of steel jacket at 78 K provide approximately a 100-dB absorption loss for a 10-kHz ambient radiation. The large attenuation has two implications with regards to the shielding effectiveness. First, the shield reduces the internal field to a level low enough to allow the operation at Dirac monopole sensitivity. This conclusion is drawn from the consistency of the Gaussian fit in Fig. 10 with the observed signal-to-noise ratio for a Dirac monopole. Second, the large attenuation factor due to the shield implies that the field level in the detector can be monitored with great sensitivity simply by crude monitoring of the external field. To eliminate the electromagnetic background, the detector can be operated in anticoincidence with a simple antenna in the vicinity of the detector. The shielding required for the transient induction detectors is thus rather simple and inexpensive. On the other hand, superconducting dc induction detectors need leak-proof superconducting shielding and rigid mechanical mounting of the detector elements to avoid spurious signals.

VII. HIGH-T_c SUPERCONDUCTORS

Superconducting materials with transition temperatures well above the liquid-nitrogen temperature have been developed recently.[17] This development opens up the possibility of very-low-loss input coils and thus higher signal-to-noise ratio (S/N) for the transient detector operating at 78 K. Since simple steel shielding and low noise FET input amplifiers seem to be adequate for a transient detector, we do not propose that the new superconductors be used for shielding or that high-T_c SQUID's be developed for amplification. Since the current due to the monopole is expected to be low, high critical current density is also not required. Lack of electrical resistance is the only desired property for the transient detectors. Although no one yet claims to be able to manufacture coils from the high-T_c ceramic superconductors, several groups are working on related problems. In this section we briefly discuss the superconducting version of the transient response induction technique. The following arguments are equally applicable to the hybrid transient detector utilizing superconducting coils either at 78 K or at 4 K.

If the copper coil used in the detector prototype were to be replaced by a superconducting coil with the same parameters, the expected value of S/N goes up to approximately 375 from 26 even with 5 Ω allowance for stray resistance at 78 K. The high value of S/N can be converted into higher unit detector area. If the detector consists of identical superconducting coils connected in a gradiometer[11,15] pattern, the S/N should be independent of the covered area to first order. The reason is as follows: the S/N, as given by Eq. (21), depends only mildly on coil parameters other than its resistance. For the superconducting case, resistance is practically negligible. If a gradiometer pattern is constructed by connecting adjacent coils with opposing polarities, the magnetic flux linked with an element of the gradiometer is canceled to first order by that of its neighboring element. This effect counters the increase in overall self-inductance L^g of the gradiometer. Also, the gradiometer total internal capacitance $C^g_{\rm int}$ decreases because of the series addition of internal capacitance of all the elements. As a result, the gradiometer self-resonant frequency $\omega^g_{\rm os}$ given by

$$\omega^g_{\rm os}=\frac{1}{\sqrt{L^g C^g_{\rm int}}} \tag{26}$$

should remain approximately the same as that of the unit coil. Since $\omega_{\rm os}$ is the only coil parameter in the S/N Eq. (21), the S/N should remain approximately the same as that of a unit coil. The gradiometer S/N remains the same as that of the unit coil to the first order provided the number of units is small. In any case, since the readout for each gradiometer would be provided by an inexpensive FET amplifier and low-frequency conventional electronics, there is no reason to demand that each gradiometer assembly cover a very large area. It thus appears that the operation of a transient detector with superconducting coil elements is feasible. It is our feeling that the transient detection method with its inexpensive steel shielding, FET amplifier and easy environment monitoring is a simpler method of detecting cosmic-ray monopoles than the conventional dc detectors with their tight superconducting shielding, SQUID-based am-

plifiers, and very sensitive environmental monitors. With the fabrication of high-T_c superconducting wire, one should be able to build induction detectors based on the transient technique as large as several 100 m^2 at a cost far below that of any other method.

VIII. CONCLUSION

We have used the Faraday induction principle to design and operate a small transient-response velocity-independent magnetic monopole detector at 78 K. Low-loss copper coils and low-noise amplifiers with high input impedance were required to achieve adequate signal-to-noise ratio (S/N). An optimal filter specific to the extraction of the monopole signal from the background of coil and amplifier thermal noise was implemented. Simple shielding with thin structural steel sheets was shown to be adequate. The observed power S/N for an 11.4-cm-diameter copper coil at liquid-nitrogen temperature was 25.9±3.1, which agrees within error limits with the S/N calculated from the coil resistivity function. The signal-to-noise figure implies a negligible false event rate for the triple coincidence operation of three small coils of this type. The S/N is sensitive to the resistive loss in the coil. With the level of loss expected for a copper coil, building very large arrays at the level of Parker flux limit for galactic monopoles with reasonable S/N may be difficult. However, with superconducting input coils, the task appears feasible. Recent spectacular developments in the field of high-T_c superconductors may allow fabrication of very low loss 78 K coils in the near future. In that case, building large area magnetic monopole detectors with inexpensive low-frequency conventional electronics, simple steel shielding, and easy environment monitoring based on the transient detection technique is a possibility.

ACKNOWLEDGMENTS

We thank our former undergraduates A. Amiry, J. Matthews, and S. Schwartz for patiently winding and testing the copper coils, M. Campbell for putting together the data-acquisition system, fellow graduate colleague P. Derwent for careful research on the low noise amplifiers, and R. Gabriel and R. Northrop for technical support. P. Boynton of the University of Washington and B. Cabrera of Stanford University were very helpful to us in early discussions. Finally, M. Kuchnir of the Fermi National Accelerator Laboratory and R. Gustafson of the University of Michigan deserve a great deal of thanks for their help on earlier aspects of this work. This research was supported by the U.S. National Science Foundation Grant No. NSF-PHY-86-01628. This work forms part of a thesis to be presented to the Department of Physics, The University of Chicago, in partial fulfillment of the requirements of the Ph.D. degree.

APPENDIX A: CURRENT DETECTION

Figure 11 shows the equivalent circuit of a sensing coil connected to a current-sensing (transimpedance) amplifier which is nothing but an inverting operational amplifier

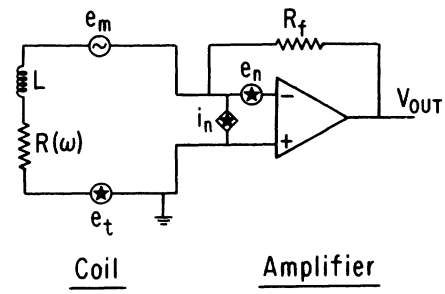

FIG. 11. Equivalent circuit of a current-sensing detector. The input coil has inductance L and resistance $R(\omega)$. The inverting amplifier voltage output V_{out} is proportional to the coil current. R_f is the feedback resistance, e_m is the monopole emf, and e_t is the coil thermal noise. e_n and i_n denote the amplifier voltage and current noise, respectively.

with negative feedback. All the parameters are as in the voltage amplifier scheme except that the capacitance is shorted by the amplifier and can be ignored. The feedback resistor R_f is held at temperature T_f. The monopole signal input current $M(t)$ is a solution of the differential equation:

$$L\frac{dM(t)}{dt}+RM(t)=e_m(t) \ . \tag{A1}$$

The Fourier transform of the above equation gives the expression for the signal in frequency space (with fast monopole approximation):

$$M(\omega)=\frac{4\pi ng}{R(\omega)+i\omega L} \quad (-\infty<\omega<\infty) \ . \tag{A2}$$

If we assume that coil resistance is a constant R, the time domain signal corresponding to Eq. (A2) is

$$\begin{aligned} M(t)&=0, \quad t\le 0 \\ &=\frac{4\pi ng}{L}e^{-Rt/L}, \quad t\ge 0 \end{aligned} \tag{A3}$$

which is the decaying step response of an RL circuit to a step input.

The current noise power spectral density $S_n(\omega)$ is the sum of four terms:

$$S_n(\omega)=S_{nt}(\omega)+S_{nv}(\omega)+S_{ni}(\omega)+S_{nf}(\omega) \ , \tag{A4}$$

where the terms on the right-hand side are the spectral densities of the coil thermal noise, the amplifier voltage noise, the amplifier current noise, and the feedback resistor thermal noise.

The first term $S_{nt}(\omega)$ is the Johnson noise spectrum $2kTR(\omega)$ modified by the RL circuit response of the coil, namely, the absolute value squared of the denominator in Eq. (A2):

$$S_{nt}(\omega)=\frac{2kTR(\omega)}{R^2(\omega)+\omega^2L^2} \quad (-\infty<\omega<\infty) \ . \tag{A5}$$

For the special case of $R(\omega)=$const, it is easy to verify that Eq. (A5) conforms to the statement of the equipartition theorem

$$\frac{1}{2\pi}\int_{-\infty}^{\infty} S_{nt}(\omega)d\omega=\frac{kT}{L} . \tag{A6}$$

In the limit of infinitely small L (i.e., the RL circuit being replaced by a resistor R), Eq. (A5) gives back the familiar expression for the white-noise current spectral density:

$$S_{nt}(\omega)=\frac{2kT}{R(\omega)} \quad (L\rightarrow 0) \quad (-\infty<\omega<\infty) . \tag{A7}$$

The second term on the right-hand side of Eq. (A4) is the amplifier input voltage noise density $S_{nv}(\omega)$. It is device dependent and is shaped by the RL circuit response. To obtain $S_{nv}(\omega)$, the output voltage due to the noise current of the amplifier is calculated. The voltage is divided by the feedback resistance R_f to factor out the gain, and the resulting expression is modified by the RL circuit response of the coil:

$$S_{nv}(\omega)=\frac{\lambda_v(\omega)(1+\omega^2L^2/R_f^2)}{R^2(\omega)+\omega^2L^2}, \quad -\infty<\omega<\infty . \tag{A8}$$

The term ω^2L^2/R_f^2 is the noise enhancement due to the feedback. It can, in general, be made negligible by choosing a large enough feedback resistance.

The third term on the right-hand side of Eq. (A4) is the amplifier current noise density:

$$S_{ni}(\omega)=\lambda_i(\omega), \quad -\infty<\omega<\infty . \tag{A9}$$

For an FET, the current noise is very small.

The fourth and final term is the thermal-current noise of the feedback resistance R_f:

$$S_{nf}(\omega)=\frac{2kT_f}{R_f}, \quad -\infty<\omega<\infty . \tag{A10}$$

The feedback noise can be made negligible by choosing a large enough feedback resistance.

Adding together only the significant current noise terms [Eqs. (A5), (A8), and (A9)] we get the total input noise-current spectrum

$$S_n(\omega)=\frac{2kT}{R(\omega)}\left[\frac{1+\chi(\omega)}{1+Q^2(\omega)}+\eta(\omega)\right], \quad -\infty<\omega<\infty , \tag{A11}$$

where the dimensionless quantities $\chi(\omega)$ and $\eta(\omega)$ representing the amplifier voltage noise and the current noise, respectively, have been defined previously [Eq. (15)].

If we ignore the amplifier noise and assume $R(\omega)$ is independent of ω, we can calculate the signal-to-noise ratio from Eqs. (A3) and (A6):

$$S/N=\frac{(4\pi g)^2}{kT}\left[\frac{n^2}{L}\right] . \tag{A12}$$

The raw S/N above is the same as that for the voltage amplifier [Eq. (16)].

As before we can use the optimal linear filter to enhance the S/N [Eq. (A12)] by a factor G_{opt}. Ignoring a term of order $Q^{-2}(\omega)$ in the denominator,

$$G_{\text{opt}}=\frac{1}{2\pi}\int_0^{\infty} Q(\omega)\frac{d\omega/\omega}{1+Q^2(\omega)\eta(\omega)+\chi(\omega)} . \tag{A13}$$

This expression for G_{opt} is very similar to the corresponding expression [Eq. (19)] for the voltage detector. The integrand above is strictly less than the one in the voltage case for frequencies less than $\sqrt{2}\,\omega_0$ where ω_0 is the resonant frequency. Although the frequency range of the integral, in principle, extends all the way to infinity, it is only an idealization of the actual upper cutoff frequency ω_c imposed by the amplifier noise or the sampling frequency, as discussed before. Since the resonant frequency ω_0 is set arbitrarily by a tuning capacitor, we can choose $\omega_0>\omega_c/\sqrt{2}$ thereby making sure that the S/N enhancement factor G_{opt} for the voltage detector is greater than that for the current sensing detector. To conclude, a properly designed voltage detector is always superior to the corresponding current detector.

APPENDIX B: LOW-LOSS COILS

In this appendix we report the results of our efforts on the design and winding of minimum-loss copper wire coils. The results are mostly empirical, with qualitative understanding of the complex mechanism of the ac resistive loss. Considering the complexity of the problem we feel that much more effort would be required to find a comprehensive solution. However, successful fabrication of high-T_c superconducting wire would be the ideal solution.

To make the notion of a low-loss coil quantitative, we first generalize the definition of the quality factor Q of a coil by extending it from a specific frequency to the entire frequency range of interest for a given application. The integrated quality factor $\langle Q\rangle$ is then defined by

$$\langle Q\rangle=\int_0^{\infty}\frac{L}{R(\omega)}d\omega , \tag{B1}$$

where L and R denote the coil inductance and resistance, respectively; ω is the angular frequency, and the integration is carried out over the frequency range of interest.

The definition of $\langle Q\rangle$ shows that a good coil maximizes the ratio of inductance to the total resistance over the frequency range. To achieve this goal, one has to consider the effects of changing the various coil design parameters. For a coil with a given diameter, a set of independent parameters would, for example, consist of the wire conductivity and diameter, winding length, number of layers, winding pitch, thickness, and finally the dielectric constant and loss coefficient of the interlayer spacing material. It is also possible to use different winding techniques aimed at reducing undesirable properties. For example, the so-called "universal winding method" can be used to reduce the net internal capacitance of the coil.

All the coils tested during the course of this study were wound using normal winding procedure. The length of each coil was made equal to the core radius and all of the layers in a coil had the same winding direction. Several precautions were taken to reduce the resistive loss of the coil. Polyethylene has a very low dielectric loss

coefficient and was used as the spacer between the layers. Usage of materials with appreciable dielectric loss such as insulating varnish, sticky tapes, etc., was kept to a minimum. The coils were baked in dry nitrogen before testing to remove all traces of moisture. It was seen repeatedly that the coil internal capacitance decreased and the coil Q increased upon baking. This behavior is consistent with the large dielectric constant and the loss coefficient of water. Low-loss polystyrene shunt capacitors were used to resonate the coil at different frequencies. All metallic objects were removed from the vicinity of the coil. All these precautions ensure that both the dielectric and stray eddy losses were small compared to the internal eddy loss of the coil. The coils were evaluated at room temperature just before the cooldown.

To measure the parameters of a coil, the coil is resonated at different frequencies by varying the external (shunt) polystyrene capacitance. The resonant frequency is noted and the Q at that frequency is measured by the method described in Appendix C. The inverse squared resonant frequency is plotted as a function of the shunt capacitance. The graph is a straight line. The slope of the line gives the coil inductance and the intercept provides the self-capacitance of the coil. The procedure is accurate to about one-tenth of 1% for the inductance and to 2% for the internal capacitance. Having estimated the coil inductance, the total resistance as a function of frequency is obtained from the known Q values at different frequencies.

Although the measurement of the coil resistance function is relatively easy, its interpretation is not. There does not appear to be any recent literature on the subject and the older literature tends to be insufficient[23] in technical detail. All the data we studied were obtained in our laboratory.

Since the ac resistance is the result of eddy loss in the conducting metal, the resistivity is expected to go up with the frequency, a fact borne out by the data. However, the extent to which the ac loss dominates over the dc loss and the characteristic frequency scale which determines the onset of the ac loss are both very sensitive to the coil parameters. It was noted that the Q always degrades when the (external) shunt capacitance is small in comparison with the (internal) self-capacitance of the coil, i.e., for frequencies close to the self-resonant frequency. All of the other coil parameters appear to be unimportant. It follows that the scaling frequency for the eddy loss must be the self-resonant frequency of the coil. Also, it is the only frequency in the system. On the other hand, the magnitude of ac loss is sensitive to the wire conductivity and its diameter. Depending on the coil design, it is possible to have a substantial increase in the total resistive loss upon cooling in spite of the eightfold decrease in the dc resistance.

Figures 12 and 13 illustrate both of the above points. The two plots show the ac component of the total resistance plotted as a function of the frequency for a 20-layer coil at room temperature and at liquid-nitrogen temperature. The wire conductivity is the only coil design parameter that is different for the two sets of data shown. The ac resistance is scaled to the dc resistance and the

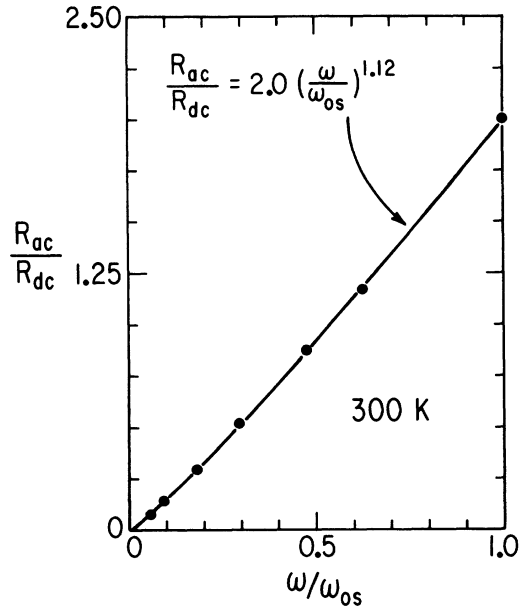

FIG. 12. ac resistance of a copper coil measured as (indicated by dots) a function of frequency for a room-temperature coil. The ac resistance for a given frequency is obtained by measuring the coil Q. The resistance is scaled to the dc resistance and the frequency is scaled to the self-resonant frequency of the coil. The curve is a power-law fit.

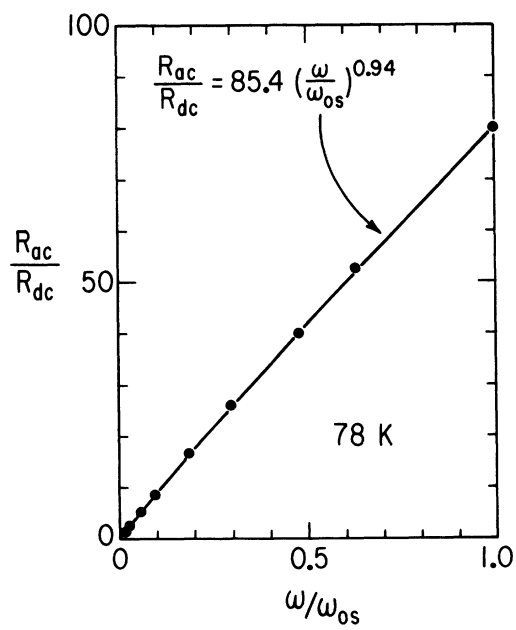

FIG. 13. ac resistance as a function of frequency for the coil in Fig. 12 after cooling it to 78 K. Conductivity is the only parameter of the coil that changes upon cooldown. Although the conductivity increases, the linear coefficient in the fit increases considerably. The overall Q of the coil is better at room temperature in spite of lower dc conductivity.

frequency is scaled to the self-resonant frequency. The shown fits are of the form

$$\frac{R_{ac}(\omega)}{R_{dc}} = \alpha \left[\frac{\omega}{\omega_{os}} \right]^{\beta}, \tag{B2}$$

where $R_{ac}(\omega)$ denotes the ac component of the resistance at frequency ω, R_{dc} is the dc resistance, and ω_{os} is the self-resonant frequency of the coil. Both α and β are dimensionless coefficients which are obtained from the fit. The coefficient β is approximately unity in most cases and varies over a small range upon changes in the coil parameters. The value of α shows wide variation from coil to coil and is fundamental to the coil loss. For example, in the case of the above coil, a change of a factor of 8 in the conductivity upon cooldown resulted in an approximate 40-fold increase in α. The total resistance changed from the dc-dominated mode at room temperature to the ac mode at the liquid-nitrogen temperature. Contrary to intuition, the total liquid-nitrogen resistance for this coil is significantly higher than the total room-temperature resistance at most frequencies. Other authors who dealt with the subject of "room temperature" monopole detectors did not take the ac loss into account.[16]

The explanation of both the above characteristics is the skin effect induced by the self-capacitance. Imagine the coil resonating at its self-resonant frequency in absence of any external capacitance. The total electromagnetic energy stored in the coil oscillates between the electric and the magnetic mode during the course of each cycle. In the magnetic mode, all the energy resides in the magnetic field produced by the current flowing through the conductor. In the electrical mode, it is stored in the electric field produced by the physical separation of the charges on the conductor. The resonance occurs as a result of the reciprocity between the separation of charges and the flow of the current. In the absence of an external tuning capacitance, the coil resonates entirely by itself. During the electrical mode of a self-resonant coil, the charges reside entirely on the coil surface. The resulting current, then, has a tendency to flow on the conductor surface. Another way of visualizing this effect is to imagine a transverse force on the charged carriers of the current due to the capacitative charge separation. Because of the surface current flow, only a part of the conductor cross section is used, resulting in net increase of the Ohmic resistance. This mechanism is very similar to that of the more common high-frequency skin effect for a straight conductor. However, for a coil, the skin effect is induced by the self-resonant frequency of the coil. Just as in the straight wire skin effect, the extent of the resistance increase is governed by the ratio of the conductor diameter to the skin depth. Equivalently, the coefficient α is a monotonically increasing function of the ratio of wire diameter to skin depth.

The exact functional dependence of α on the ratio of the wire diameter to the skin depth is as yet unknown. Considering the size of the phase space spanned by the multitude of coil design parameters, empirical evaluation of this function appears to be difficult. Since the recent advent of high-T_c superconductors presents the possibility of building very-low-loss coils, there does not seem to be much point in pursuing this difficult task.

APPENDIX C: Q MEASUREMENT FOR LOW LOSS COILS

In this appendix we outline and justify a procedure used to measure the Q of low-loss coils. Conventional Q measurement methods involve loading the coil, thereby degrading its Q. The solution to the problem is to excite the coil by minimal magnetic coupling and also to measure the coil response in the same manner.

The coil is magnetically coupled to a few turns of an excitation loop and also to a similar pickup loop. Let M_e and M_p denote the mutual inductance between the coil and excitation loop, and the coil and pickup loop, respectively. The pickup and excitation loops should be as far apart as possible to avoid direct coupling between them. The coil is excited by applying voltage V at frequency ω across the excitation coil and the voltage V_{out} across the pickup loop is fed to an oscilloscope using a low-capacitance attenuator probe. A high input impedance low-noise voltage amplifier may be required to amplify the output. The equivalent electrical circuit of the coil with measurement setup is shown in Fig. 14. By scanning through the frequency range, the resonant frequency ω_0 and the full frequency width at half the resonant voltage response, $\Delta\omega$, are measured. The coil Q is then given by

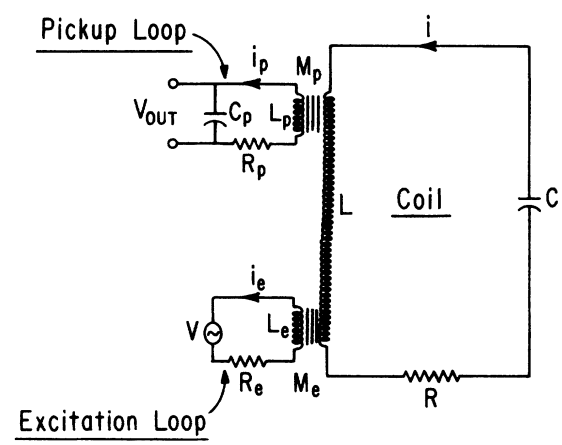

FIG. 14. The equivalent circuit of the Q measurement setup. In this procedure, resonant loading of the coil is minimized, allowing measurement of very high Q's. Subscripts e and p refer to the excitation and pickup loops, respectively. The number of turns in each of these loops is very small compared to that in the coil. Typically, they have two or three turns.

$$Q(\omega_0)=\sqrt{3}\left[\frac{\omega_0}{\Delta\omega}\right] . \tag{C1}$$

To justify this equation and to obtain the conditions of validity we need to analyze the circuit of Fig. 14, i.e., obtain the output voltage in terms of the input voltage.

The circuit equations are

$$V=L_e\frac{di_e}{dt}+R_e i_e-M_e\frac{di}{dt} , \tag{C2}$$

$$M_e\frac{di_e}{dt}=L\frac{di}{dt}+Ri+\frac{\int i\,dt}{C}-M_p\frac{di_p}{dt} , \tag{C3}$$

$$M_p\frac{di}{dt}=L_p\frac{di_p}{dt}+R_p i_p+\frac{\int i_p dt}{Cp} , \tag{C4}$$

$$V_{\text{out}}=\frac{\int i_p dt}{Cp} . \tag{C5}$$

Assuming sinusoidal forms for all variables, the parameters i_e, i, and i_p can be eliminated from Eqs. (C2), (C3), (C4), and (C5), and we are left with the output voltage in terms of the input voltage:

$$\left|\frac{V_{\text{out}}}{V}\right|=\frac{M_e M_p}{R_e}\frac{\omega_0}{L}\frac{\left[\frac{\omega}{\omega_0}\right]^3}{\left\{\left[1-\left[\frac{\omega}{\omega_0}\right]^2\right]^2+\frac{1}{Q^2}\left[\frac{\omega}{\omega_0}\right]^4\right\}^{1/2}} , \tag{C6}$$

where ω_p is the resonant frequency of the pickup loop, $Q_e=R_e/\omega L_e$, and we assumed $\omega_0 \ll \omega_p$ and $Q \ll Q_e$. The first of the two conditions is trivial to satisfy since the pickup loop has very small inductance and capacitance which makes ω_p much larger than the coil-resonant frequency ω_0. The second condition $Q \ll Q_e$ requires that the excitation circuit be a very stiff current source. A stiff current source prevents the severe resonant loading from changing the supply current in the excitation circuit. Q_e sets the upper limit on the Q that can be measured using a given measurement setup. Q_e cannot be made infinitely large without making the output voltage vanishingly small. It is seen from Eq. (C6) that for constant input voltage, the output voltage as a function of frequency depends only on the coil Q and the resonant frequency ω_0, apart from the multiplicative constants. It is easy to show from this expression that ω_0 and Q are given by the full-width-at-half-maximum expression of Eq. (C1).

---

*Present address: EP Division, CERN, CH-1211, Geneva 23, Switzerland.

[1]G. 't Hooft, Nucl. Phys. **B79**, 276 (1974); A. M. Polyakov, Pis'ma Zh. Eksp. Teor. Fiz. **20**, 430 (1974) [JETP Lett. **20**, 194 (1974)].

[2]The standard big-bang model of the Universe has an overabundance of monopoles, see J. Preskill, Phys. Rev. Lett. **43**, 1365 (1979); A. H. Guth and S. H. Tye, *ibid.* **44**, 631 (1980). The "inflationary" model of the early Universe reduces the monopole abundance by proposing that the Universe underwent a very rapid expansion when it was small and uniform. The inflation scenario seems to predate grand unified monopoles. (E. B. Gliner, Pis'ma Zh. Eksp. Teor. Fiz. **22**, 378 (1966) [JETP Lett. **22**, 245 (1966)].) The monopole abundance problem was the motivation for a crucial step in the development of inflation in 1981 by Guth, see A. H. Guth, Phys. Rev. D **23**, 347 (1981). However, the Universe in this scenario became too inhomogeneous. The "new inflation" [A. D. Linde, Phys. Lett. **108B**, 389 (1982); A. Albrecht and P. J. Steinhardt, Phys. Rev. Lett. **48**, 1220 (1982)] solved the inhomogeneity problem. For the theory of thermal production of monopoles in the inflationary scenario, see W. Collins and M. S. Turner, Phys. Rev. D **29**, 2158 (1984); P. R. Lindblom and P. J. Steinhardt, *ibid.* **31**, 2151 (1985). For the current status of the inflation theory, see R. H. Brandenberger, *Inflation and Cosmic Strings* (World Scientific, Singapore, 1987).

[3]Over the years, people have tried to look for monopoles produced in accelerators. For example, H. Bradner and W. M. Isbel, Phys. Rev. **114**, 603 (1959); M. Fidecaro *et al.*, Nuovo Cimento **22**, 657 (1961); E. M. Purcell *et al.*, Phys. Rev. **129**, 2326 (1963); R. A. Carrigan, Jr., F. A. Nezrick, and B. P. Strauss, Phys. Rev. D **8**, 3717 (1973); D. M. Stevens *et al.*, *ibid.* **14**, 2207 (1976); R. A. Carrigan, Jr., B. P. Strauss, and G. Giacomelli, *ibid.* **17**, 1754 (1978); D. Fryberger, T. E. Coan, K. Kinoshita, and P. B. Price, *ibid.* **29**, 1524 (1984); P. Musset, M. Price, and E. Lohrmann, Phys. Lett. **128B**, 333 (1983); B. Aubert, P. Musset, M. Price, and J. P. Vialle, *ibid.* **120B**, 465 (1983).

[4]W. V. R. Malkus, Ph.D. thesis, University of Chicago, June 1950; W. V. R. Malkus, Phys. Rev. **83**, 899 (1951); Malkus also tried to collect light cosmic-ray monopoles using laboratory magnetic fields; also, see R. L. Fleischer, P. B. Price, and R. T. Woods, *ibid.* **184**, 1398 (1969), for a monopole track search.

[5]The theory of excitation of simple atoms by slow-moving massive monopoles was developed by Drell and co-workers; S. Drell, N. Kroll, M. Mueller, S. Parke, and M. Ruderman, Phys. Rev. Lett. **50**, 644 (1983); monopole search experiments have been done based on this technique; for example, see F. Kajino, S. Matsuno, Y. K. Yuan, and T. Kitamura, *ibid.* **52**, 1373 (1984); T. Hara *et al.*, *ibid.* **56**, 553 (1986); G. E. Masek *et al.*, Phys. Rev. D **35**, 2758 (1987) (UCSD Helium proportional tubes search).

[6]Ahlen and Kinoshita calculated the ionizing power of slow-moving monopoles; S. P. Ahlen and K. Kinoshita, Phys. Rev. D **26**, 2347 (1982). Slow protons have been used to measure

ionizing power at low velocities (Ref. 13). Several experiments have reported null results based on ionization. E. N. Alexeyev, M. M. Boliev, A. E. Chudakov, and S. P. Mikehyev, in *Proceedings of the Nineteenth International Cosmic Ray Conference,* La Jolla, California, 1985 edited by F. C. Jones, L. Adams, and G. M. Mason (NASA Conf. Publ. No. 2376) (Goddard Space Flight Center, Greenbelt, MD, 1985), Vol. 8, p. 250 (Baksan Collaboration has the leading upper limit on monopole flux among the non-Faraday induction experiments); M. Aglietta *et al.*, Nuovo Cimento **9C**, 588 (1986) (Mont Blanc liquid-scintillation detector experiment); G. Battistoni *et al.*, *ibid.* **9C**, 551 (1986) (Monte Blanc NUSEX experiment); J. Bartelt *et al.*, Phys. Rev. D **36**, 1990 (1987) (Soudan-1 detector); T. M. Liss, Ph.D. thesis, University of California, Berkeley, 1984; for a good description of the technique and experiments, see T. M. Liss, S. P. Ahlen, and G. Tarlé, Phys. Rev. D **30**, 884 (1984). For monopole flux limit from lack of tracks in ancient mica, see P. B. Price and M. H. Salamon, Phys. Rev. Lett. **56**, 1226 (1986); also see Ref. 14.

[7]Alvarez, and later Tassie were the first to propose the use of superconducting loops for monopole search; L. W. Alvarez, LBL Physics Note No. 470, 1963; L. J. Tassie, Nuovo Cimento **38**, 1935 (1965). The size of the monopole signal was calculated by Eberhard and collaborators; P. H. Eberhard, R. N. Ross, L. W. Alvarez, and R. D. Watt, Phys. Rev. D **4**, 3260 (1971). The first induction detector was used to look for monopoles in moon rocks; see L. W. Alvarez, proposal to NASA, 1966. The first use of SQUID's is credited to Vant-Hull; L. L. Vant-Hull, Phys. Rev. **173**, 1412 (1968).

[8]The monopoles are expected to catalyze baryon decay by Callan-Rubakov effect: V. A. Rubakov, Pis'ma Zh. Eksp. Teor. Fiz. **33**, 658 (1981) [JETP Lett. **33**, 644 (1981)]; Nucl. Phys. **B203**, 311 (1982); C. G. Callan, Jr., Phys. Rev. D **26**, 2058 (1982). As a result, proton-decay experiments can also place an upper limit on the product of the monopole flux and the catalysis cross section, see J. Stone *et al.*, Nucl. Phys. **B252**, 261 (1985). Also see S. Errede, in *Monopole '83,* proceedings, Ann Arbor, Michigan, 1983, edited by J. L. Stone (NATO Advanced Study Institute, Series B: Physics, Vol. 111) (Plenum, New York, 1984), p. 169; W. J. Marciano and D. Salvino, in *Proceedings of the Summer Study on the Physics of the Superconducting Super Collider,* Snowmass, Colorado, 1986, edited by R. Donaldson and J. Marx (Division of Particles and Fields of the APS, New York, 1987); A. S. Goldhaber, S. Nussinov, and L. Stodolsky, Nucl. Phys. **B296**, 955 (1988). Assuming baryon catalysis, the observed properties of neutron stars and pulsars also impose monopole flux limits. E. W. Kolb, S. A. Colgate, and J. A. Harvey, Phys. Rev. Lett. **49**, 1373 (1982); K. Freese, M. S. Turner, and D. N. Schramm, *ibid.* **51**, 245 (1983).

[9]E. N. Parker, Astrophys. J. **163**, 225 (1971).

[10]M. S. Turner, E. N. Parker, and T. J. Bogdan, Phys. Rev. D **26** (1982).

[11]M. E. Huber, B. Cabrera, M. A. Taber, and R. D. Gardner, IEEE Trans. Magn. MAG-23 **2**, 1134 (1987); M. E. Huber, B. Cabrera, M. A. Taber, and R. D. Gardner, Jpn. J. Appl. Phys. **26**, 1687 (1987) (the Stanford group); S. Bermon, IEEE Trans. Magn. MAG-23 **2**, 441 (1987); S. Bermon, P. Chaudhari, C. C. Chi, C. D. Tesche, and C. C. Tsuei, Phys. Rev. Lett. **55**, 1850 (1985) (the IBM group). These two groups have the leading monopole flux limits based on Faraday induction.

[12]P. B. Price *et al.*, Phys. Rev. Lett. **35**, 487 (1975); B. Cabrera, *ibid.* **48**, 1378 (1982); A. D. Caplin, C. N. Guy, M. Hardiman, J. G. Park, and J. C. Schouten, Nature (London) **317**, 234 (1985).

[13]Assuming that the ionizing power of slow monopoles is at least equal to that of equal velocity protons (Ref. 6), the velocity dependence of monopole ionization power can be measured at accelerators; see S. P. Ahlen, T. M. Liss, C. Lane, and G. Liu, Phys. Rev. Lett. **55**, 181 (1985).

[14]The Baksan Collaboration (in Ref. 6) already has an ionization detector operating at the level of the Parker limit. The MACRO Collaboration [G. Tarlé *et al.*, Report No. CALT-68-1292b, 1985 (unpublished)] is building a big monopole detector in the Gran Sasso tunnel in Italy. The search technique is based on the expectation that the monopoles interact with matter.

[15]M. W. Cromer, A. F. Clark, and F. R. Ficket, Phys. Rev. Lett. **56**, 2561 (1987) (NBS Group); J. Incandela, H. Frisch, S. Somalwar, M. Kuchnir, and H. R. Gustafson, Phys. Rev. D **34**, 2637 (1986) (the Chicago-Fermilab-Michigan group); T. Ebisu and T. Watanabe, J. Phys. G **11**, 883 (1985) (monopoles trapped in iron ore).

[16]M. J. Price, in *Monopole '83* (Ref. 8), seems to be the only published work on nonsuperconducting detection of monopoles. Also see C. Rubbia, E. P. Internal Report No. 82-01, CERN, Geneva; D. E. Morris's work as described by C. C. Tsuei, in *Monopole '82,* edited by R. Carrigan, Jr. and W. P. Trower (Plenum, New York, 1983).

[17]*Proceedings of the Symposium on High Temperature Superconductors,* edited by D. U. Gubser and M. Schluter (Materials Research Society, Pittsburgh, 1987), Vol. EA-11.

[18]The usual expression for the thermal noise has an extra factor of 2 because normally only the positive frequencies are taken into account.

[19]F. W. Grover, *Inductance Calculations* (Van Nostrand, New York, 1946).

[20]L. A. Wainstein and V. D. Zubakov, *Extraction of Signal from Noise* (Prentice-Hall, Englewood Cliffs, 1962).

[21]Aliasing: when an analog signal is made discrete by sampling, the sampled data contains frequencies only below the half-sampling frequency (Nyquist sampling theorem). The higher-frequency components, if present in the signal, contaminate the data by appearing as additional lower-frequency components. This phenomenon is called aliasing. Analog low-pass filtering before digitzation prevents aliasing.

[22]Data Translation, Inc., 100 Locke Drive, Marlborough, MA 01752.

[23]V. G. Welsby, *The Theory and Design of Inductance Coils* (Wiley, London, 1960).